

## Suredaite, $\text{PbSnS}_3$ , a new mineral species, from the Pirquitas Ag-Sn deposit, NW-Argentina: mineralogy and crystal structure

WERNER H. PAAR,<sup>1</sup> RONALD MILETICH,<sup>2,6</sup> DAN TOPA,<sup>3</sup> ALAN J. CRIDDLE,<sup>4</sup>  
MILKA K. DE BRODTKORB,<sup>5</sup> GEORG AMTHAUER,<sup>1</sup> AND GEROLD TIPPELT<sup>1</sup>

<sup>1</sup>Institut für Mineralogie, Universität Salzburg, Hellbrunnerstrasse 34, A-5020 Salzburg, Austria

<sup>2</sup>Laboratory for Crystallography, ETH Zürich, Sonneggstrasse 5, CH-8092 Zürich, Switzerland

<sup>3</sup>Institute of Geology and Paleontology, Universität Salzburg, Hellbrunnerstrasse 34, 5020 Salzburg, Austria

<sup>4</sup>Department of Mineralogy, The Natural History Museum, London SW7 5BD, U.K.

<sup>5</sup>Consejo Nacional de Investigaciones Científicas y Técnicas—University of Buenos Aires, Paso 258-9A, 1640 Martinez, Argentina

<sup>6</sup>Bayerisches Geoinstitut, Universität Bayreuth, D-95445 Bayreuth, Germany

### ABSTRACT

Suredaite, ideally  $\text{PbSnS}_3$ , is a new mineral species from the Pirquitas Ag-Sn deposit (Province Jujuy, NW-Argentina). It was observed in symmetrically banded veins in the Oploca district, and is associated with sphalerite, arsenopyrite, pyrite-marcasite, cassiterite, cylindrite, franckeite, hocartite, rhodostannite, and various Ag-Sb and Ag-Bi sulfosalts in minor amounts. Suredaite occurs in layers up to 1 cm in thickness as aggregates of radially arranged tabular-prismatic (single) crystals, has a metallic lustre, and a dark grey streak.  $\text{VHN}_{50}$  ranges between 18.2 and 20.6 (mean 19.6) GPa, the Mohs hardness is 2.5–3. It has perfect cleavages parallel to  $\{001\}$ ,  $\{101\}$ , and  $\{100\}$ . The measured density varies between 5.54 and 5.88  $\text{g/cm}^3$ ,  $D_x$  was determined to be 5.615  $\text{g/cm}^3$ . In reflected plane-polarised light, it is white and is not perceptibly bireflectant or pleochroic. It lacks internal reflections and is weakly anisotropic with metallic blue, mauve to brown rotation tints. Specular reflectance percentages in air and in oil are tabulated from 400 to 700 nm and compared graphically with those for the type specimen of teallite,  $\text{PbSnS}_2$ . Electron microprobe analyses showed suredaite to be chemically inhomogeneous with respect to the compositional variations (in wt%): Pb 42.3–48.5, Ag 0.3–1.1, Fe 0.3–1.0, As 0.2–2.1, Sn 27.7–30.2, S 23.1–24.7. The crystal structure determined from single-crystal X-ray diffraction data revealed orthorhombic symmetry [space group  $Pnma$ ,  $Z = 4$ ,  $a = 8.8221(3)$ ,  $b = 3.7728(3)$ ,  $c = 14.0076(3)$  Å;  $V = 466.23(4)$  Å<sup>3</sup>]. The atomic arrangement is isostructural to the  $\text{NH}_4\text{CdCl}_3$  structure type which exists in a series of isotypic sulfides and selenide compounds. The suredaite structure, which is the natural analogue of synthetic  $\text{PbSnS}_3$ , consists of columns of double-edge sharing octahedra running parallel to the  $b$  axis, which house the Sn atoms. These columns are linked by rods of eightfold-coordinated Pb atoms. On the basis of the structure determination, the empirically determined idealized formula follows a <sup>181</sup>(Pb, As, Ag, Sn) <sup>161</sup>(Sn, Fe)S<sub>3</sub> stoichiometry. Crystalchemical arguments suggest Ag possibly to occupy interstitial sites according to the alternative formula <sup>141</sup>(□, Ag) <sup>181</sup>(Pb, As, Sn) <sup>161</sup>(Sn, Fe) S<sub>3</sub>. The name of this new mineral species is in honor of R.J. Sureda Leston, head of the Department of Mineralogy and Economic Geology, University of Salta, Argentina.

### INTRODUCTION

Suredaite is a new tin-bearing species, which represents a valuable tin ore at Pirquitas, Argentina. It occurs in an unique mineral assemblage, which is composed of the arsenic-substituted derivatives of franckeite and cylindrite. Both represent new mineral species currently under investigation. The new mineral is named for Ricardo Sureda Leston, Professor of Mineralogy and Economic Geology at the University of Salta, NW-Argentina, for his significant contributions to the mineralogy and metallogeny of NW-Argentina. Holotype material is deposited under catalog numbers 14389-14391 in the reference

collection of the Institute of Mineralogy (University of Salzburg) and cotype (BM 1998, 39-40) in the collections of the Natural History Museum (London).

### LOCATION AND GENERAL GEOLOGY

The Pirquitas mining district is located in the Puna 135 km west of Abra Pampa, Province of Jujuy, NW-Argentina (Coira and Brodtkorb 1995; Sureda et al. 1986; Turner 1982). The mineralization is genetically comparable to the Ag-Sn formation of Bolivia and is the southernmost representative of this economically very important mineral belt. The district of Pirquitas includes the primary Ag-Sn deposit and alluvial tin and gold accumulations that were exploited intermittently from 1936 to 1990. Recently performed exploration drilling lead to

\*E-mail: werner.paar@sbg.ac.at

a preliminary resource of 118 million ounces of silver and 40 000 tonnes of tin (Anonymous 1997).

The vein system, which is hosted by Ordovician marine pelites and sandstones of the Acoyte Formation, is exposed in an area of 1.5 times 2 km. The more important veins are Oploca, Potosí, San Pedro, San Miguel, Llallagua, and Chocaya (Fig. 1). The high-grade mineralization of the Oploca and Potosí systems occurs as bundles of parallel, WNW-ESE trending extensional veins and veinlets in the hinge zone of the Cerro San Pedro anticlinal structure. At San Miguel a more stockwork type of Ag-Sn mineralization has recently been established by exploration drilling. The mineralization of the veins is polymetallic and was precipitated in several superimposed pulses, commonly recognized as telescoping in this deposit type (Malvicini 1978).

At Oploca a great variety of different mineral associations occurs, particularly in deeply interpenetrating textures. The common species are pyrite, marcasite, arsenopyrite, cassiterite; stannite, hocartite, rhodostannite; franckeite, wurtzite, sphalerite; freibergite, pyrargyrite, and miargyrite. The less common are chalcopyrite, pavonite, benjaminite, matildite, potosiite, cylindrite, and incaite. The minor phases are ferberite, diaphorite, andorite IV and VI, ramdohrite, fizelyite, kesterite, ferrokesterite, pirquitasite, toyohaite, canfieldite, Te-canfieldite, tetradymite, and petrukite. The trace constituents are sakuraiite, native gold, and other unidentified minerals. The results of a detailed mineralogical study using electron microprobe and X-ray diffraction techniques are reported by Paar et al. (1996).

### THE SUREDAITE LOCATION

The vein containing suredaite and another as yet unnamed new mineral species (a Pb-Sn-As-S compound) is part of the Oploca vein system in the SW corner of the Pirquitas ore field (Fig. 1). This system is exposed in the Oploca crosscut, level

2, which is situated at 4250 m above sea level. Two major veins are important at this level: the suredaite vein at 315 m and the hocartite vein some 322 m distance from the entrance of the crosscut.

The suredaite vein follows an east-west trending extensional structure, which is exposed for some 100 m from the intersection of the crosscut and the structure. Suredaite occurs only to the east of the intersection, whereas to the west it is missing and franckeite predominates. The suredaite-containing vein ranges in thickness from 0.3 to 0.4 m and is exposed for 10–12 m in the roof of the gallery. The vein shows all the characteristic features of open space filling, such as symmetrical banding, crustification, vugs etc. (Fig. 2a).

The depositional sequence (Fig. 2a) is characterized by an early crystallization of franckeite associated with cylindrite, hocartite, rhodostannite, and minor amounts of various Ag-Sb and Ag-Bi sulfosalts belonging to the andorite group, lillianite as well as pavonite homologous series. It is followed by the formation of sphalerite with large embedded crystals of suredaite, and then by a repeated precipitation of As-rich franckeite, suredaite in massive layers, and sphalerite. As-rich franckeite and sphalerite always show colloform textures and are volumetrically the most abundant phases. The microparagenesis of a typical suredaite layer is demonstrated in Figure 2b.

The other vein, the hocartite vein, is exposed south of the suredaite vein, and was extensively mined for Ag and Sn. The main silver minerals in that vein are members of the hocartite-pirquitasite solid solution series, which occur as massive bands up to several cm, rarely in crystals up to several mm, in association with pyrite, marcasite, sphalerite-wurtzite, stannite-kesterite, ferrokesterite and traces of various other sulfides and sulphosalts. A channel sample taken between 312 and 331 meters of the crosscut yielded for that section 1.6% (or 527 ounces) of Ag (!) and 0.857% Sn!

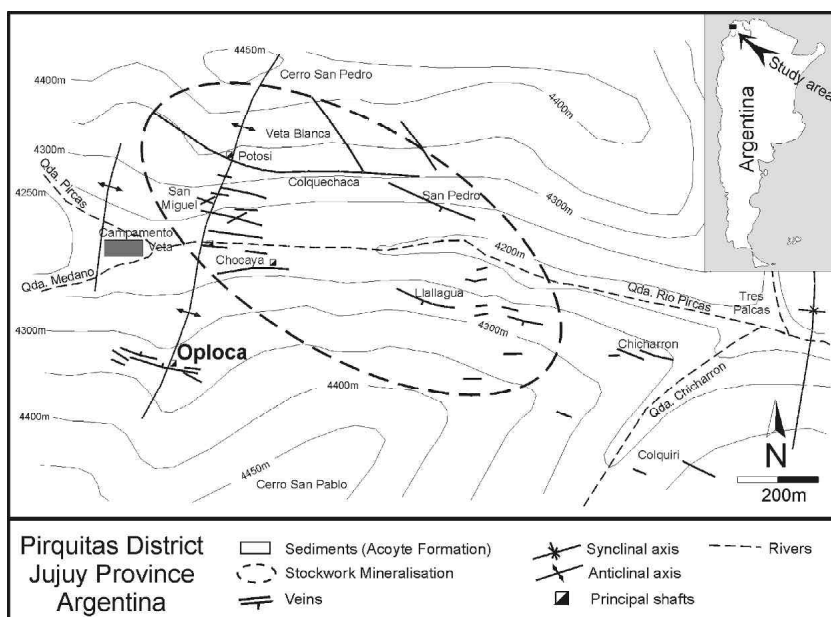


**FIGURE 1.** Geological map of the Pirquitas vein district showing important structures and the location of the stockwork mineralization. The Oploca vein section, source of suredaite, is situated in the SW corner of the district.

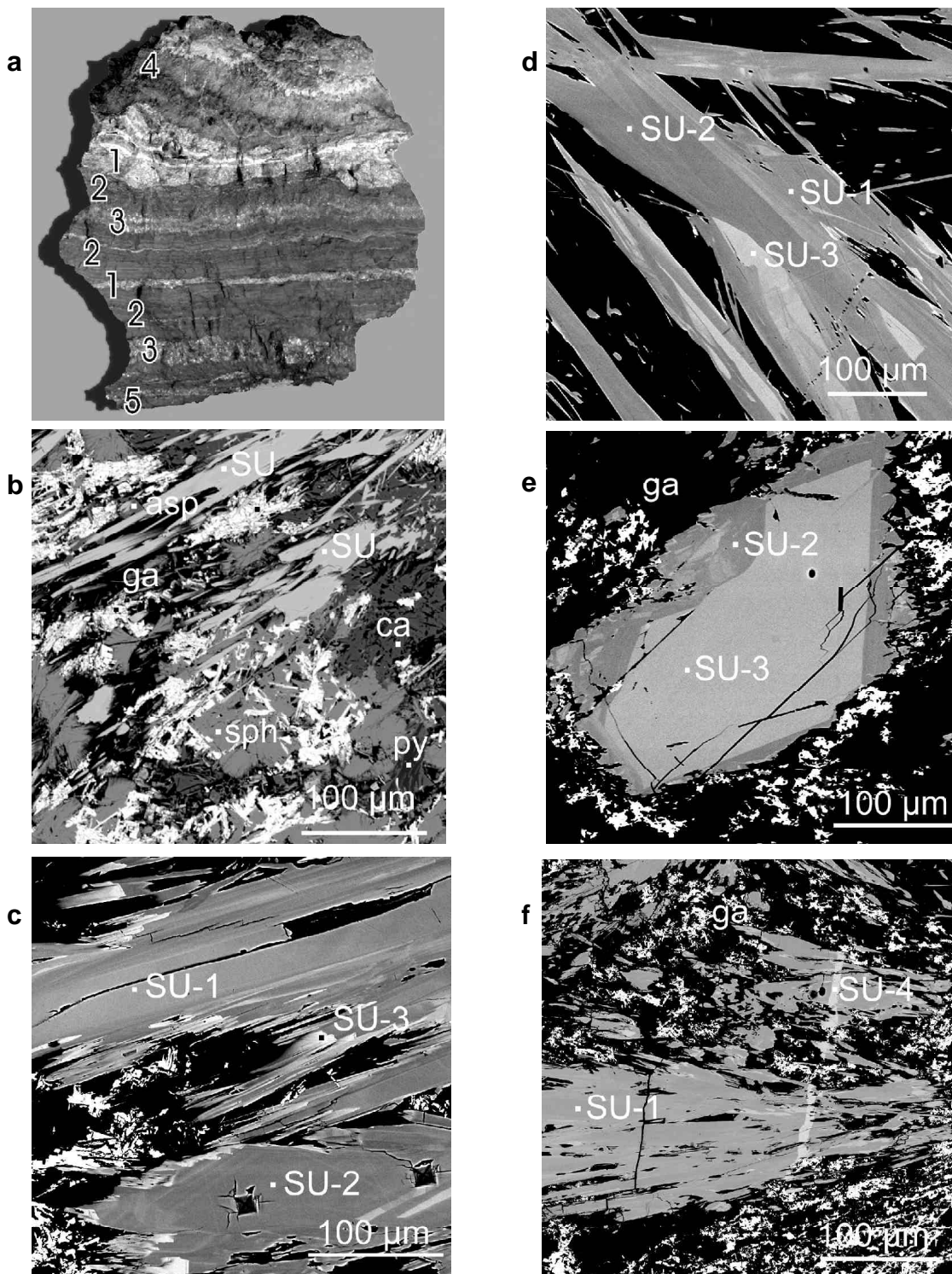


**FIGURE 2.** (a) Symmetrical banding of a typical suredaite-bearing specimen from the suredaite vein, Oploca vein (level 2). The numbers are for 1 sphalerite, 2 As-rich franckeite, 3 suredaite (massive), 4 suredaite + sphalerite (single crystals), 5 franckeite. (b) Elongated tablets of suredaite (SU) embedded in sphalerite (sph), which is intergrown with cassiterite (ca). Skeletal galena (ga) and minor amounts of pyrite/marcasite (py) and arsenopyrite (asp) (not discernible in this image) are characteristic associates of the suredaite paragenesis. (c and d) Crystals of suredaite displaying chemical variations indicated by different shades of gray in the image. Two cleavages (parallel to the elongation and perpendicular to it) are also shown. (e) BSE image of a large single crystal of suredaite (typ 2), chemically SU-3, surrounded (replaced) by SU-2. White is skeletal galena. (f) Veinlet of SU-4 crosscutting SU-1; ga is galena.

### APPEARANCE AND PHYSICAL PROPERTIES

Suredaite has an overall appearance very much resembling teallite, PbSnS<sub>2</sub>, which is a relatively common constituent in tin deposits of Bolivia, but a very rare species in Pirquitas. Suredaite was almost certainly mistaken for teallite in earlier descriptions of the deposit (Malvicini 1978).

Suredaite occurs (1) as layers up to 1 cm thickness which are composed of tubular prismatic crystals, elongated along [010] and intergrown in fan-shaped arrangements, and (2) as individual euhedral almost needle-like crystals, embedded in sphalerite. The color is grayish-black with a metallic luster and a black streak. Suredaite has perfect cleavages parallel {001}, {101}, and {100}.

The Mohs hardness is 2.5–3, the VHN<sub>50</sub> measured on {h01} from 20 indentations ranges between 18.2–20.6, mean 19.6 GPa. The indentations were obtained with a Leitz Miniload 2 hardness tester and have a straight shape with traces of cleavage cracks being created (Fig. 2c). The density was measured with a Berman microbalance on several hand-picked fragments ranging in the weight from 8.4 to 12.8 mg. The results vary between 5.54 and 5.88 g/cm<sup>3</sup> depending on the presence of other intimately intergrown sulfide phases (Fig. 2b). The calculated density, assuming a molecular weight of 395.4 for suredaite, which is the weighted average of the chemically differing varieties SU1 through 4 (Table 1), and Z = 4, gave 5.615 g/cm<sup>3</sup>.

### OPTICAL PROPERTIES

In polished section in plane-polarized light, suredaite appears white compared with the associated sphalerite. Although acicular in form, it is not apparently birefractant or pleochroic, however it is anisotropic, and between crossed polars its characteristic rotation tints are metallic blue to mauve to brown. It is opaque, has straight extinction, and within the visible spectrum lacks internal reflections. Reflectance measurements were made from 400 to 700 nm using Zeiss MPM800 spectrophoto-

meter, and a WTiC standard on freshly polished grains: ×50 air and oil objectives, effective NA 0.3 were used for measurement. The measured field was 15 μm in diameter. These, together with color values calculated from them relative to the CIE illuminant C are tabulated (Table 2). They are characteristic and do not match any of the spectra in the reflectance databases of Criddle and Stanley (1993) or Picot and Johan (1982). The opportunity was taken to compare the type specimen of the superficially similar mineral teallite. This sample, BM 86482, from Bolivia was described by Prior (1904). A polished section was prepared and measured under the same conditions as described for suredaite. Teallite is significantly higher reflecting in air and in oil than suredaite (Fig. 3) and its spectra are differently dispersed. In fact, the reflectance spectra of teallite when compared with data in the QDF (Criddle and Stanley 1993) are closer to those of herzenbergite, SnS, than to those of suredaite. This is not surprising since herzenbergite has been reported as forming a solid solution series with teallite (Chang and Brice 1971).

### ELECTRON MICROPROBE ANALYSES

Several sections prepared from the original (holotype) specimen and material from the suredaite vein were investigated using a JEOL Superprobe JXA-8600 with an ELX-Link system at 25 kV and 30 nA, installed at the Institute of Geology and Paleontology (University Salzburg). Natural PbS (galena) (PbMα, SKα) and FeAsS (arsenopyrite) (FeKα, AsLα) as well as synthetic Ag and Sn (AgLα, SnLα) were used as standards. The raw data were processed with the LINK ZAF-4 program. The results are presented in Table 1. A special problem turned out to be the overlap of the PbMα and AsKα lines. Due to peak overlap, the small arsenic content was not detected in the preliminary analyses that were used in the abstract submitted for approval to the IMA CNMMN.

Suredaite is chemically inhomogeneous and the variation

TABLE 1. Electron microprobe analyses of suredaite

Sample		Pb	Ag	Fe	As	Sn	S	Total	EF‡
SU-1	61*	42.27	0.80	0.77	1.41	30.12	24.23	99.60	70
	sd†	0.67	0.09	0.10	0.17	0.26	0.19	0.72	
	min	41.29	0.57	0.52	0.95	29.56	23.77	98.50	
	max	43.93	0.99	0.93	1.74	30.81	24.72	101.20	
SU-2	29	41.05	1.10	1.03	2.11	30.24	24.68	100.22	20
	sd	0.53	0.12	0.11	0.18	0.39	0.26	0.52	
	min	40.22	0.91	0.75	1.76	29.66	24.10	98.82	
	max	42.15	1.34	1.22	2.37	30.96	25.18	101.01	
SU-3	30	46.05	0.49	0.61	0.56	28.66	23.71	100.08	9
	sd	0.55	0.16	0.15	0.19	0.46	0.21	0.50	
	min	45.11	0.20	0.16	0.25	27.56	23.25	99.22	
	max	46.94	0.73	0.79	0.82	29.76	24.13	101.23	
SU-4	12	48.50	0.27	0.26	0.21	27.74	23.14	100.11	1
	sd	0.62	0.20	0.16	0.10	0.45	0.39	0.51	
	min	47.32	0.00	0.06	0.08	26.97	22.34	99.28	
	max	49.00	0.50	0.51	0.41	28.30	23.68	100.80	
<b>atomic proportions (S = 3)</b>									
SU-1		0.809	0.029	0.055	0.075	1.007			
SU-2		0.772	0.039	0.072	0.110	0.993			
SU-3		0.901	0.018	0.044	0.030	0.980			
SU-4		0.973	0.010	0.019	0.012	0.972			

\* Mean value of (N) analyses.

† Standard deviation.

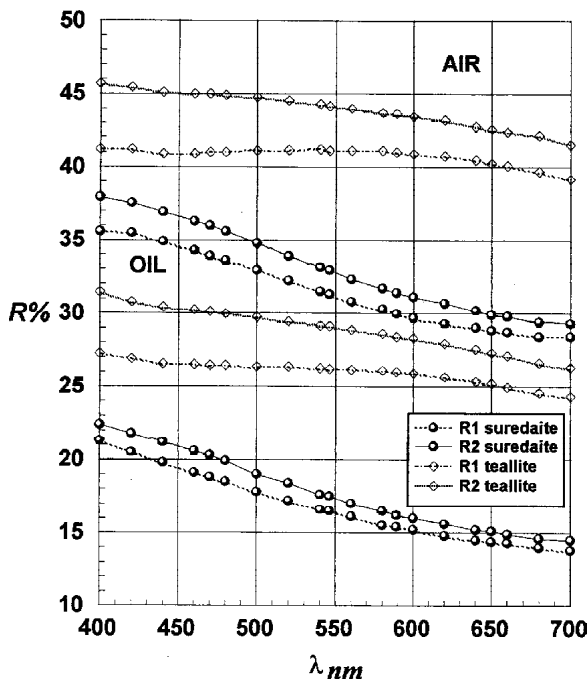
‡ Estimated frequency (%).

**TABLE 2.** Reflectance data and color values for suredaite

$\lambda_{nm}$	$R_1\%$	$R_2\%$	$^mR_1\%$	$^mR_2\%$
400	35.6	37.9	21.3	22.4
420	35.5	37.5	20.5	21.8
440	34.0	36.9	19.8	21.2
460	34.3	36.3	19.1	20.6
480	33.6	35.6	18.5	19.9
500	32.9	34.8	17.8	19.0
520	32.2	33.9	17.2	18.4
540	31.5	33.1	16.6	17.6
560	30.8	32.3	16.1	17.0
580	30.3	31.7	15.5	16.5
600	29.7	31.1	15.2	16.0
620	29.3	30.7	14.8	15.6
640	29.0	30.2	14.5	15.2
660	28.7	29.8	14.3	14.9
680	28.4	29.4	14.0	14.6
700	28.4	29.3	13.8	14.5

**Colorvalues: CIE Illuminant C**

x	0.297	0.296	0.289	0.287
y	0.304	0.304	0.296	0.295
Y%	31.1	32.6	16.3	17.3
$\lambda_d$	479	479	478	478
$P_e\%$	6.1	6.6	10.0	10.7

**FIGURE 3.** Specular reflectance spectra in air and in oil ( $N_D = 1.515$ ) for suredaite and teallite.

of the elements is given in Table 1. A distinct zonation occasionally can be recognized in the BSE images (Figs. 2c–2e), with a general tendency of the Pb-enriched varieties to form the outer rims of the crystals (Fig. 2c). A more irregular distribution of SU-3 can be noted in Figure 2d, with a general tendency to form the more central portions of the crystals. The reverse trend can be observed in the large suredaite crystals, which are embedded in sphalerite (Fig. 2e). SU-4 is supposedly the latest in the crystallization sequence of all suredaite

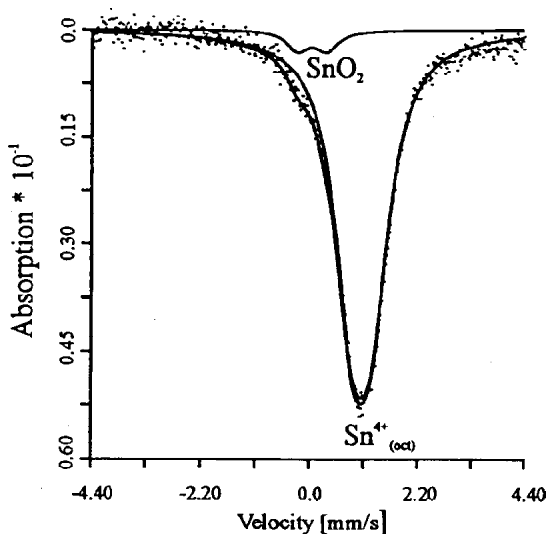
chemical varieties. It forms rare crosscutting veinlets in SU-1 (Fig. 2f).

**MÖSSBAUER SPECTROSCOPY**

Mössbauer spectra of  $^{119}\text{Sn}$  in suredaite were taken in transmission at 298 K absorber temperature using a conventional Mössbauer spectrometer (Halder electronic, Germany) in horizontal arrangement, a 10 mCi  $\text{CaSnO}_3$ -source at room temperature, a constant acceleration drive system with symmetric triangular velocity shape, and a multichannel analyzer with 1024 channels. The velocity range was within 4.40 mm/s and the velocity scale was calibrated by an  $\alpha\text{-Fe}$  foil. The two mirror image spectra obtained (512 channels each) were folded and evaluated with symmetric doublets with Lorentzian line shape using the program MOESALZ (Lottermoser et al. 1993). Isomer shifts are reported relative to  $\text{SnO}_2$  at room temperature.

The main feature in the Mössbauer spectrum of  $^{119}\text{Sn}$  in suredaite (Fig. 4) is a strong line at about 1.00 mm/s. This line was evaluated by a quadrupole split doublet with an isomer shift of 1.06 mm/s, a quadrupole splitting of 0.39 mm/s, and with an area of 95% of the total resonant absorption area, and is assigned without any doubt to  $\text{Sn}^{4+}$  in octahedral  $S^{2-}$ -coordination. The measured isomer shift is very close to the isomer shift of 1.13 mm/s of octahedrally coordinated  $\text{Sn}^{4+}$  in  $\text{Sn}_2\text{S}_3$  (Amthauer et al. 1979). The comparatively small half width of 0.88 mm/s points to the occupation of just one crystallographic position by  $\text{Sn}^{4+}$ . The small quadrupole splitting indicates only a minor distortion of the  $\text{SnS}_6$ -polyhedron. There are no indications of significant amounts of  $\text{Sn}^{2+}$  in the spectrum. An additional doublet with very low intensity (5.00% of the total resonant absorption area) and centered at 0.03 mm/s has to be fitted to the spectrum. This minor subspectrum is assigned to  $\text{SnO}_2$ -inclusions in the suredaite matrix.

$^{57}\text{Fe}$  spectra of the suredaite sample were also taken with the same spectrometer but using a  $^{57}\text{Co}$  in Rh source. However,

**FIGURE 4.** Mössbauer spectrum of  $^{119}\text{Sn}$  in suredaite.

due to the very low iron content (0.3–1.0 wt%) and the strongly absorbing ions, such as Pb and Sn, in the compound, the <sup>57</sup>Fe-spectrum is of poor quality and cannot be evaluated accurately. Nevertheless, a tentative interpretation of the <sup>57</sup>Fe-spectrum yields 2 weak doublets with almost equal areas, which are assigned to almost equal amounts of Fe<sup>2+</sup> and Fe<sup>3+</sup> in octahedral environment. The Fe<sup>2+</sup> doublet may be due to inclusions of Fe<sup>2+</sup>-bearing sulfides, such as sphalerite, (Zn,Fe)S, pyrite, FeS<sub>2</sub>, marcasite, FeS<sub>2</sub>, and arsenopyrite, FeAsS.

### X-RAY CRYSTALLOGRAPHY

Samples of suredaite were investigated both by powder and single-crystal X-ray diffraction. X-ray powder diffraction measurements were performed on a SIEMENS D5000 diffractometer with a flat specimen mounted on a silicon single-crystal sample holder using CuK $\alpha$  radiation. The powder diffraction pattern (Table 3) was recorded with 0.02° steps and 9 s counting time per step in the range 5–100° 2 $\theta$ . The majority of the reflections could be indexed on the basis of a primitive orthorhombic unit cell. Final lattice parameters are:  $a = 8.8213(7)$  Å,  $b = 3.7725(3)$  Å, and  $c = 14.0053(9)$  Å, which were obtained from a constrained least-squares fit to 70 accurate 2 $\theta$  values using NBS Si added as an internal standard to the samples. The determination of peak positions, the fitting of peak profiles, the peak-position calibration, and the final refinements of the unit-cell parameters were performed with the software package VISUAL-X<sup>POW</sup> (Stoe and Cie 1994). The powder diffraction pattern also contained peaks from minor amounts of ZnS and three peaks from a yet unidentified phase.

A  $4.2 \times 10^{-5}$  mm<sup>3</sup> (20  $\mu$ m  $\times$  20  $\mu$ m  $\times$  105  $\mu$ m) irregular crystal fragment was selected for the single-crystal X-ray diffraction investigation. X-ray intensities were collected on an Enraf Nonius CAD4 four-circle diffractometer using graphite-monochromatized MoK $\alpha$  radiation from an X-ray tube operated at 50 kV and 50 mA. The intensity measurements of all symmetry-allowed reflections ( $0 \leq h \leq 14$ ;  $0 \leq k \leq 6$ ;  $-22 \leq l \leq 22$ ) were collected with  $2\theta$ - $\omega$ -scans for  $2\theta \leq 70^\circ$ . Integrated X-ray intensities were obtained from the scan data using a modified Lehmann-Larsen algorithm (Grant and Gabe 1978). Intensities were corrected for Lorentz and polarization effects and crystal absorption by Gaussian integration according to the crystal shape ( $\mu_{\text{MoK}\alpha} = 428.3$  cm<sup>-1</sup>) using a modified version of the program ABSORB (Burnham 1966). Data reduction confirmed the absence conditions for *Pnma* space-group symmetry. Averaged structure factors were obtained by averaging symmetry equivalent reflections in Laue group *mmm* following the averaging criteria recommended by Blessing (1987). A structure solution was obtained by direct methods with the SIR program package (Altomare et al. 1994) confirming the structural model proposed for synthetic PbSnS<sub>3</sub> (Jumas et al. 1972). Subsequent refinements were carried out with RFINE90, a development version of RFINE4 (Finger and Prince 1975) using the atomic coordinates given by Jumas et al. (1972) for the starting model. The coefficients for scattering factors of neutral atoms and the coefficients for dispersion corrections were taken from the *International Tables for Crystallography* (Maslen et al. 1992; Creagh and McAuley 1992). The final refinements were carried out with anisotropic displacement pa-

TABLE 3. X-ray powder diffraction data for suredaite

$hkl(\times 100)$	$d_{\text{obs}}$ (Å)	$d_{\text{calc}}$ (Å)	$hkl$
2.1	7.452	7.464	1 0 1
1.4	6.993	7.003	0 0 2
26.4	5.483	5.485	1 0 2
9.0	4.408	4.411	2 0 0
100.0	4.128	4.126	1 0 3
30.0	3.730	3.732	2 0 2
7.1	3.645	3.643	0 1 1
15.0	3.3672	3.3669	1 1 1
13.9	3.2545	3.2544	1 0 4
19.4	3.2051	3.2061	2 0 3
27.6	3.1085	3.1082	1 1 2
7.9	2.9299	2.9342	0 1 3
9.1	2.8811	2.8777	3 0 1
14.6	2.8689	2.8669	2 1 0
50.8	2.8081	2.8086	2 1 1
40.9	2.7421	2.7423	2 0 4
4.1	2.7114	2.7111	3 0 2
51.1	2.6692	2.6697	1 0 5
18.8	2.6518	2.6531	2 1 2
10.6	2.4872	2.4880	3 0 3
12.3	2.4651	2.4642	1 1 4
3.1	2.4428	2.4430	2 1 3
15.5	2.3648	2.3645	2 0 5
16.5	2.3342	2.3342	0 0 6
13.3	2.2474	2.2489	0 1 5
2.1	2.2180	2.2182	2 1 4
4.3	2.2027	2.2016	3 1 2
20.9	2.1037	2.1035	4 0 2
21.8	2.0634	2.0631	2 0 6
3.0	2.0287	2.0281	3 0 5
3.9	2.0041	2.0035	2 1 5
5.2	1.9942	1.9940	4 0 3
11.6	1.9507	1.9512	1 0 7
53.5	1.9335	1.9335	3 1 4
19.0	1.8866	1.8865	4 1 1
5.7	1.8367	1.8372	4 1 2
6.0	1.8225	1.8221	2 0 7
10.0	1.7839	1.7837	1 2 2
9.8	1.7506	1.7507	0 0 8
12.2	1.7152	1.7155	1 2 3
3.7	1.6836	1.6834	2 2 2
6.5	1.6508	1.6503	5 0 3
14.5	1.6410	1.6407	2 1 7
38.9*	1.6316	1.6319	1 2 4
7.0	1.6030	1.6030	4 0 6
6.0	1.5777	1.5775	3 2 1
15.2	1.5629	1.5629	1 1 8
6.5	1.5582	1.5581	5 1 2
4.4	1.4189	1.4198	1 1 9
4.3	1.4048	1.4043	4 2 2
11.3	1.3795	1.3792	4 1 7
26.5	1.3754	1.3754	3 0 9
3.2	1.3682	1.3677	2 1 9
6.5	1.3262	1.3266	4 2 4
2.6*	1.3015	1.3018	6 0 5
8.0	1.2987	1.2987	1 1 10
3.2	1.2604	1.2602	1 0 11
15.0*	1.2418	1.2420	5 2 3
2.0	1.2307	1.2306	6 1 5
1.3	1.1918	1.1917	2 3 2
5.3	1.1802	1.1803	5 1 8
3.6	1.1707	1.1706	5 2 5
3.1	1.1592	1.1596	6 2 0
5.7	1.1282	1.1283	2 0 12
3.5	1.1152	1.1149	5 1 9
9.9	1.1113	1.1113	3 2 9
20.7*	1.1086	1.1089	7 0 6
3.3	1.0984	1.0984	1 3 6
9.7	1.0451	1.0449	7 2 1

Note: Equipment: SIEMENS D5000 powder diffractometer, CuK $\alpha$  radiation, Peltier-cooled silicon detector; scan range 5–100° 2 $\theta$ , 0.02° steps, 9 s counting time per step; peak positions corrected for NBS Si internal diffraction standard ( $a = 5.43088$  Å); 70 indexed reflections,  $\Delta(2\theta)_{\text{max}} = 0.047^\circ$ ; additional lines of ZnS and three lines of yet unknown phase eliminated from pattern; intensities derived from peak fitting procedure.

\* Intensities probably overestimated due to overlap with ZnS lines

rameters for all atoms. A correction for secondary isotropic extinction (Lorentzian type I distribution, Becker and Coppens 1974) resulted in insignificant values and was therefore omitted from the final refinement. Details of the data collection, the data reduction, and the refinements are given in Table 4, the resulting positional parameters and displacement parameters are listed in Table 5, and bond distances and angles are given in Table 6.

Unit-cell parameters were determined using a customized HUBER four-circle diffractometer operated with unmonochromatized Mo X-ray radiation; details of the diffractometer and the centering procedure are given in Angel et al. (1997). Reflection centering was carried out with fixed 6 mm × 1 mm slit sizes that respectively define the diffracted-beam divergence within the 2θ plane and perpendicular to it. To prevent crystal-offset errors and diffractometer aberrations affecting the results, the technique of diffracted-beam centering (King and Finger 1979) was employed to obtain correct setting angles. The unconstrained refinement of the unit-cell parameters corresponds, within their uncertainties, to orthorhombic symmetry. The refinement constrained to orthorhombic symmetry by a vector-least-squares fit (Ralph and Finger 1982) to 41 corrected reflection positions within the 7.4–23.4° range in 2θ yielded:  $a = 8.8221(3)$ ,  $b = 3.7728(3)$ ,  $c = 14.0076(3)$  Å.

### CRYSTAL STRUCTURE DESCRIPTION

The structure of suredaite (Fig. 5) was found to consist of double columns of edge-sharing octahedra, mostly of Sn atoms (= B site), linked together by eightfold-coordinated Pb atoms (= A site). Not only the octahedrally coordinated atoms are arranged in columns but also the eightfold-coordinated Pb atoms form columns by sharing common edges (Fig. 6). Both

**TABLE 4.** Details of the intensity measurement, the data reduction, and results of the refinements

Scan range	(°)	1.00 + 0.35 tanθ
Scan time	(s)	12 to 120
Background	(°)	2×0.16
Total  F	(+h, +k, ±l)	2260
Averaged  F	(F > 0σ)	1131
F  <sub>obs</sub>	(F > 4σ)	244
R <sub>int</sub> (F <sub>obs</sub> )		0.039
μ(MoKα)	(cm <sup>-1</sup> )	428.3
Transmission factors	(%)	38.2 to 55.6
N <sub>var</sub>		33
R		0.054
wR	(w = [σ <sup>2</sup> + 0.0006 F <sup>2</sup> ] <sup>-2</sup> )	0.048
G <sub>fit</sub>		0.94
ΔF /σ(F)		≤ 1.7

Notes:  $R = [\sum w(|F_o| - |F_c|)] / \sum F_o$ ;  $G_{fit} = [\sum w(|F_o| - |F_c|)^2 / (N_{obs} - N_{var})]^{1/2}$ .

**TABLE 5.** Fractional coordinates and displacement parameters for suredaite (Pb,As,Ag,Sn)(Sn,Fe)S<sub>3</sub> (Pnma, Z = 4)

Atom	x/a	y/b	z/c	β <sub>11</sub>	β <sub>22</sub>	β <sub>33</sub>	β <sub>13</sub>	B <sub>eq</sub>
A*	0.5030(4)	0.75	0.1705(2)	0.0109(4)	0.0269(15)	0.0034(2)	-0.0001(3)	2.54
B*	0.1655(5)	0.25	0.0521(3)	0.0037(4)	0.0223(28)	0.0014(2)	0.0002(3)	1.16
S1	-0.0114(18)	0.75	0.1062(9)	0.0063(19)	0.017(8)	0.0015(7)	-0.0014(13)	1.39
S2	0.3394(14)	0.75	-0.0066(9)	0.0012(11)	0.031(9)	0.0013(7)	-0.0006(10)	1.06
S3	0.2855(16)	0.25	0.2132(9)	0.0075(18)	0.015(8)	0.0016(7)	-0.0020(10)	1.51

Note: All atoms on site 4c (site symmetry: . m .); β<sub>12</sub> = β<sub>23</sub> = 0; estimated standard deviations are given in parentheses; anisotropic displacement parameters are given in the form exp[-(h<sup>2</sup>β<sub>11</sub> + k<sup>2</sup>β<sub>22</sub> + l<sup>2</sup>β<sub>33</sub> + 2hlβ<sub>13</sub>)].

\* Refined site occupancy: Pb<sub>0.92(2)</sub>Sn<sub>0.08(2)</sub>.

† Refined site occupancy: Sn<sub>0.99(2)</sub>Fe<sub>0.01(2)</sub>.

**TABLE 6.** Selected interatomic distances (Å) and bond angles (°) in suredaite

A-S3 <sup>iii</sup>	2×	2.756(11)	B-S3 <sup>i</sup>		2.493(14)
A-S2 <sup>i</sup>		2.870(13)	B-S1 <sup>i,iii</sup>	2×	2.563(11)
A-S1 <sup>iv</sup>		3.130(13)	B-S2 <sup>ii,iii</sup>	2×	2.567(9)
A-S2 <sup>vii</sup>	2×	3.281(11)	B-S1 <sup>vi</sup>		2.601(4)
A-S3 <sup>iv,v</sup>	2×	3.525(12)	B...B <sup>vi,viii</sup>	2×	3.770(5)
A...A <sup>ii,iii</sup>	2×	3.773(5)	B...B <sup>ii,iii</sup>	2×	3.773(5)
A...B <sup>ii</sup>	2×	3.895(5)			
S3 <sup>i</sup> -A-S3 <sup>ii</sup>		86.4(3)	S3 <sup>i</sup> -B-S1 <sup>i,iii</sup>	2×	89.5(4)
S3 <sup>iii</sup> -A-S2 <sup>i</sup>	2×	80.7(4)	S3 <sup>i</sup> -B-S2 <sup>ii,iii</sup>	2×	92.1(4)
S3 <sup>iii</sup> -A-S1 <sup>iv</sup>	2×	5.8(4)	S1 <sup>vi</sup> -B-S1 <sup>i,iii</sup>	2×	86.2(4)
S2 <sup>i</sup> -A-S1 <sup>iv</sup>		147.5(4)	S1 <sup>vi</sup> -B-S2 <sup>ii,iii</sup>	2×	92.3(4)
S2 <sup>vi</sup> -A-S2 <sup>vii</sup>		70.2(2)	S1 <sup>i</sup> -B-S1 <sup>vi</sup>		94.8(4)
S2 <sup>vi,iii</sup> -A-S3 <sup>iv,v</sup>	2×	73.5(3)	S1 <sup>i,iii</sup> -B-S2 <sup>ii,iii</sup>	2×	85.3(3)
S2 <sup>vi,iii</sup> -A-S3 <sup>iv,v</sup>	2×	109.4(3)	S2 <sup>i</sup> -B-S2 <sup>ii</sup>		94.6(3)
S3 <sup>iv</sup> -A-S3 <sup>v</sup>		64.7(2)	S3 <sup>i</sup> -B-S1 <sup>vi</sup>		173.6(5)
S1 <sup>iv</sup> -A-S3 <sup>iv,v</sup>	2×	64.3(3)	S1 <sup>i,iii</sup> -B-S2 <sup>ii,iii</sup>	2×	178.5(5)
S2 <sup>i</sup> -A-S2 <sup>vi,iii</sup>	2×	66.9(3)			
S3 <sup>iii</sup> -A-S2 <sup>vi,iii</sup>	2×	93.1(3)			
S3 <sup>iii</sup> -A-S3 <sup>iv,v</sup>	2×	91.5(3)			

Notes: Symmetry code: i = x, y, z; ii = x, y + 1, z; iii = x, y - 1, z; iv = 1/2 + x, y, 1/2 - z; v = 1/2 + x, y + 1, 1/2 - z; vi = -x, -y, -z; vii = -x, -y + 1, -z; viii = -x, -y - 1, -z.

the (Sn<sub>2</sub>S<sub>6</sub>)<sub>n</sub> and (Pb<sub>2</sub>S<sub>8</sub>)<sub>n</sub> columns run parallel to the crystallographic b axis. The atomic arrangement was found to be isotopic to a number of synthetic ternary chalcogenides ABX<sub>3</sub> (X = S, Se) which are strongly related to the NH<sub>4</sub>CdCl<sub>3</sub> aristotype structure (Brasseur and Pauling 1938; type E 24; structure reports). Isostructural atomic arrangements in sulfides and selenides are reported for: Sn<sub>2</sub>S<sub>3</sub> (Kniep et al. 1982; Mootz and Puhl 1967), PbSnS<sub>3</sub> (Jumas et al. 1972), ABS<sub>3</sub> (A = Pb, Sn; B = Zr, Hf; Lielieveld and Ijdo 1978; Wieggers et al. 1989; Meetsma et al. 1993), Sn(Ti<sub>0.8</sub>Sn<sub>0.2</sub>)S<sub>3</sub> (Gressier et al. 1987), SbBS<sub>3</sub> (B = Cr, In; Paulus and Fuess 1992; Jobic et al. 1994), ACrSe<sub>3</sub> (A = La, Ce, Ga; Huy-Dung et al. 1971; Lutz et al. 1988) and EuZrSe<sub>3</sub> (Mar and Ibers 1992). A number of isostructural halogenides (X = Cl, Br, I) is reported in Kniep et al. (1982).

The coordination of the A site in suredaite can be described as a bicapped trigonal prism with the two triangular S<sub>2</sub>S<sub>2</sub> bases lying parallel to the (010) plane direction. The coordination polyhedron can also be described as a distorted tetragonal antiprism with S1S2S<sub>3</sub> and S2<sub>2</sub>S<sub>3</sub> defining the square bases. The central cation occupies a remarkably asymmetric position within this polyhedron being displaced off-center along the pseudo-tetrad of the square antiprism toward the S1S2S<sub>3</sub> base. Accordingly the four shortest distances (2 × 2.75, 1 × 2.87, 1 × 3.13 Å) of the A atom are those to the S atoms of the S1S2S<sub>3</sub> base whereas the four longest A-S distances (2 × 3.28, 2 × 3.52 Å) display bonding to the opposite S<sub>2</sub>S<sub>3</sub> base (Table 6). The B cations are coordinated octahedrally by six sulfur atoms with

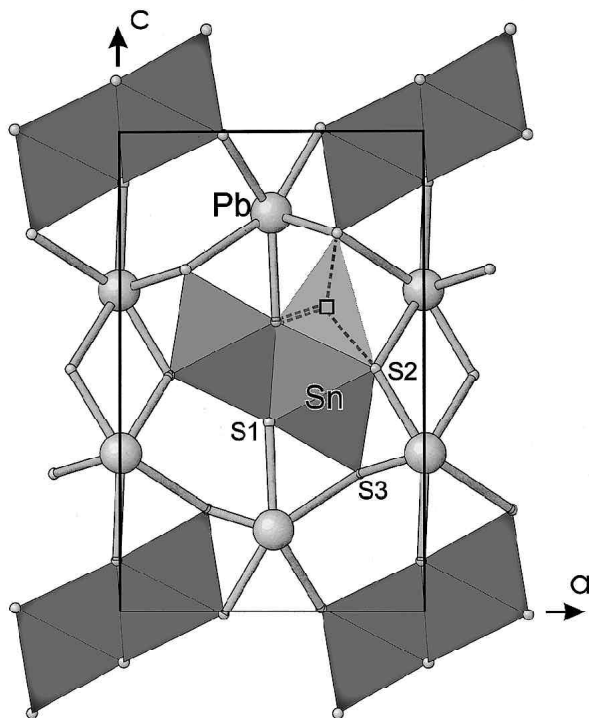


**FIGURE 5.** Crystal structure of suredaite projected down the  $b$  axis. Octahedra represent  $\text{Sn}_6$  polyhedra, large spheres are Pb atoms, and small spheres represent the S atoms.  $\square$  marks the tetrahedrally coordinated interstitial  $^{141}\square, \text{Ag}$  position which is likely to accommodate the small Ag contents.

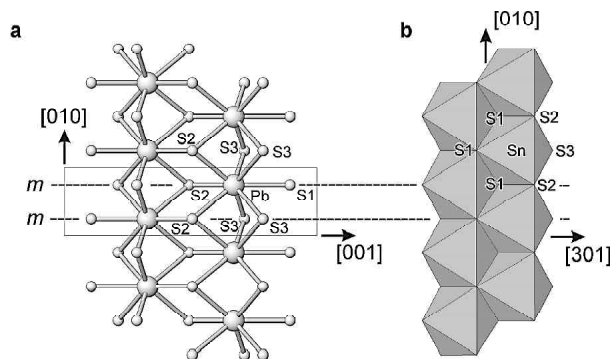


**FIGURE 6.** (a)  $[\text{Pb}_2\text{S}_8]_n$  chain in a projection down the  $a$  axis, (b)  $[\text{Sn}_2\text{S}_6]_n$  columns in a projection on (10-3). Dashed lines represent mirror planes ( $m$ ) parallel to (010) at  $y/b = 1/4$  and  $3/4$ .

B-S distances ranging from 2.49 to 2.60 Å. The three crystallographically independent S atoms are coordinated by four to six A and B cations.

### CRYSTAL CHEMISTRY

According to the microprobe analyses (Table 1) suredaite contains small but significant amounts of As [up to 0.12 atoms per formula unit (apfu)], Fe (up to 0.09 apfu), and Ag (up to

0.05 apfu) in addition to the major constituents Pb (0.77 to 1.02 apfu), Sn (0.95 to 1.03 apfu), and S (2.98 to 3.01 apfu). Compositional variation for suredaite was found in particular for the minor constituents (As, Fe, Ag) and the lead contents in contrast to the tin and sulfur contents which are close to ideal 1 and 3 atoms per formula unit. Plotting the As, Fe, and Ag contents vs. the Pb + Sn (Fig. 7) reveals that the amount of all these minor constituents increases as the number of major constituents, in particular of the Pb atoms, decreases. According to the Mössbauer spectroscopy investigations all Sn appears to be tetravalent, whereas the valency of Fe in suredaite can not be assigned without doubt. Cation distribution appears at first glance to be rather complicated, but consideration concerning the stereochemistry and charge balance lead to two possible models, of which one involves a fraction of Sn to be divalent, the other model suggests Ag on an interstitial tetrahedral site.

For both models the iron atoms can be assigned for substitution on the octahedrally coordinated B site as indicated through the Mössbauer results. The substitution of the relatively small  $\text{As}^{3+}$  for  $\text{Pb}^{2+}$  on the eightfold-coordinated A site appears to be unlikely from atomic size arguments, but the large off-center displacement reported for this site in isostructural compounds allows cations, which show a typical lone-pair effect (such as  $\text{Sn}^{2+}$ ,  $\text{Sb}^{3+}$ , or  $\text{As}^{3+}$ ), to be accommodated on this site. The off-center displacement, which occurs almost parallel to the crystallographic  $a$  direction, is responsible for a continuous transformation from a regular eightfold toward an asymmetric [3 + 5] coordination in the suredaite structure. The polyhedral distortion, as determined by the differences in bond lengths, increases significantly as the magnitude of displacement from the central position increases (Table 7). Accordingly, the  $x/a$  positional parameter, which is most sensitive to the off-center displacement, can be correlated with the distortion parameter  $\Delta$ . As shown in Figure 8 the suredaite  $x/a$ - $\Delta$  data fit on a tie line between the  $\text{Sn}_2\text{S}_3$  and  $\text{PbSnS}_3$  line indicating partial substitution of Pb on the A site by cations with a stereochemical lone-pair effect which is stronger relative to that of Pb. As previously recognized by Wiegiers et al. (1989) the degree of asymmetry of this coordination is larger for Sn than for Pb atoms due to the more covalent character of the Sn-S bond relative to that of the Pb-S bond. Evidence for a theoretically possible  $\text{Pb}^{2+} \leftrightarrow \text{Sn}^{2+}$  substitution on the A site is given by the fact that a continuous series of  $\text{PbSnS}_3$ - $\text{Sn}_2\text{S}_3$  solid solutions has been reported to exist (Pütz 1979). Furthermore, the shape, orientation, and size of the vibrational ellipsoid obtained from the anisotropic displacement parameters for the A site, which represents the average site of all cations in this refinement, support the proposed substitution mechanism of lone-pair cations and their positional differences relative to the Pb atoms on this site.

Charge-balance calculations, based on an assumption of a simple  $\text{ABS}_3$  stoichiometry, suggest the presence of a significant fraction of up to ~12%  $\text{Sn}^{2+}$  out of total Sn, even though there is no evidence for significant amounts of divalent Sn given through the Mössbauer investigations. It is remarkable that, independent on the varying amount of the minor constituents As, Fe, and Ag, the total Sn content is constant displaying almost ideal 1 apfu. Assuming the Fe to substitute for the Sn at

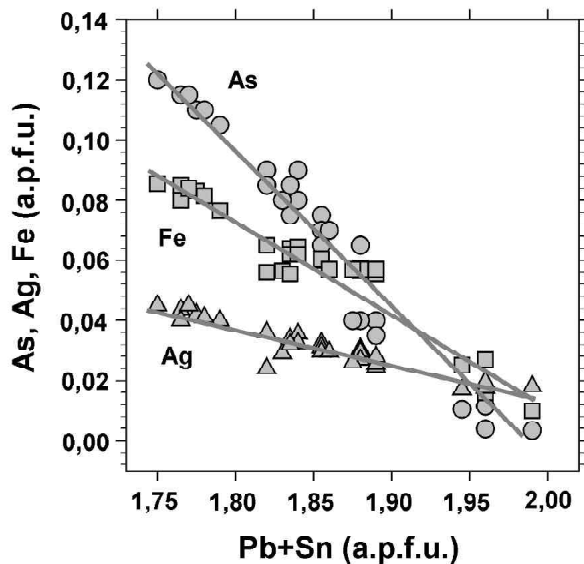


FIGURE 7. Ag, Fe, As contents in suredaites as function of Pb + Sn. Lines represent linear fits to data with unit weights.

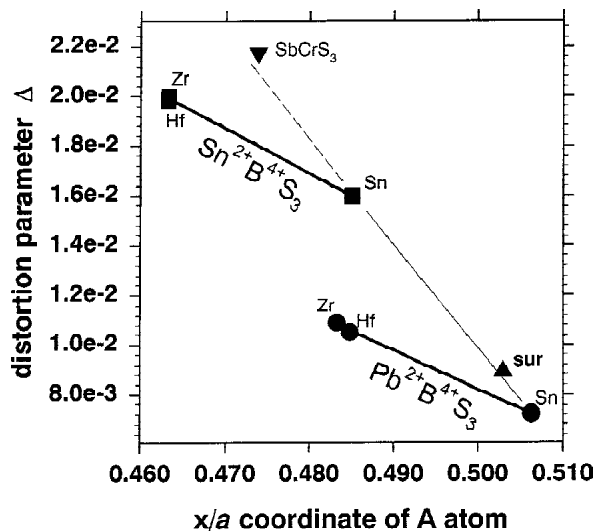


FIGURE 8. Mean square bond-length distortion parameter  $\Delta$  of the AS<sub>3</sub> polyhedron vs. fractional coordinate  $x/a$  of the A atom in A<sup>2+</sup>B<sup>4+</sup>S<sub>3</sub> compounds (A = Sn, Pb; B = Sn, Zr, Hf), Sb<sup>3+</sup>Cr<sup>3+</sup>S<sub>3</sub>, and suredaites (sur). Estimated standard deviation of the values for both  $\Delta$  and  $x/a$  are smaller than the chosen symbol size.

the B site, both the excess number of cations on the B site ( $\text{Sn} + \text{Fe} \leq 1.08$  apfu) and the deficiency on the A site ( $\text{Pb} + \text{As} \geq 0.88$  apfu) support this model of cation distribution, which suggests a simplified crystal-chemical formula  $^{18}(\text{Pb}, \text{As}, \text{Sn}^{2+}, \text{Ag})^{16}(\text{Sn}^{4+}, \text{Fe}) \text{S}_3$ . From the crystal chemistry point of view it is remarkable that: (1) the As contents (0 to 0.12 apfu) correspond almost exactly to 50% of the Pb deficiency; (2) the Fe contents are almost twice the Ag content; (3) the total Sn (=  $\text{Sn}^{2+} + \text{Sn}^{4+}$ ) approximates ideal 1 apfu. On the basis of these observations it can be calculated that the amount of Ag has to be one third of the As content for non-deficiency and complete charge compensation. Analyses confirm this 1:3 ratio (Table 1, Fig. 7) and finally lead to the empirically determined idealized formula

$(\text{Pb}_{1-6x}^{2+}\text{As}_{3x}^{3+}\text{Ag}_x\text{Sn}_{2x}^{2+})(\text{Sn}_{1-2x}^{4+}\text{Fe}_{2x}^{3+})\text{S}_3$  for this model.

On the other hand, the proposed substitution of Ag for Pb in the bicapped trigonal prism is problematic from stereochemical point of view because Ag usually prefers distorted octahedral or irregular tetrahedral environments. The existence of tetrahedral voids between the Pb prisms (Fig. 5), which are suitable in size to accommodate Ag cations, suggests to consider an alternative model with Ag on interstitial tetrahedrally coordinated site according to the empirical formula  $^{14}(\square, \text{Ag})^{18}(\text{Pb}, \text{As}, \text{Sn}^{2+})^{16}(\text{Sn}^{4+}, \text{Fe}) \text{S}_3$ . Neither a careful investigation of the electron-density map nor a structure refinement including interstitial Ag on this site yielded indications that would have verified this model.

TABLE 7. Lattice parameters (Å), mean bond lengths (Å), mean square bond-length distortion parameters  $\Delta$ , and fractional coordinates for A<sup>2+</sup>B<sup>4+</sup>S<sub>3</sub> compounds (A = Pb, Sn; B = Sn, Zr, Hf), SbCrS<sub>3</sub> and suredaites

Ref.	Sur (1)	Pb-Sn (2)	Pb-Zr (3)	Pb-Hf (4)	Sn-Sn (5)	Sn-Zr (6)	Sn-Hf (4)	Sb-Cr (7)
a	8.8221	8.738	9.013	8.988	8.878	9.188	9.139	8.665
b	3.7728	3.792	3.766	3.739	3.751	3.717	3.694	3.619
c	14.0076	14.052	13.924	13.924	14.020	13.839	13.875	12.872
<b>A site</b>								
$x/a$	0.5030	0.5063	0.4833	0.48485	0.48509	0.46328	0.46324	0.4738
$z/c$	0.1705	0.1729	0.1739	0.17411	0.16936	0.17150	0.17150	0.1608
$\Delta \times 10^{-2}$	3.1405	3.1421	3.1711	3.1620	3.1556	3.1893	3.1862	3.0211
	0.89	0.72	1.09	1.05	1.60	2.00	1.98	2.17
<b>B site</b>								
$\Delta \times 10^{-4}$	2.5590	2.5565	2.5658	2.5478	2.5638	2.5633	2.5470	2.4217
	1.97	2.63	2.45	1.75	2.06	1.07	1.29	2.32

Notes:  $\Delta = 1/n \sum [(d - \langle d \rangle / \langle d \rangle)^2]$ ,  $n$  = coordination number,  $d$  = bond distance (Brown and Shannon, 1973).

References: (1) this work; (2) Jumas et al., 1972; (3) Lelieveld and Ijdo (1978); (4) Wiegiers et al. (1989); (5) Kniep et al. (1982); (6) Meetsma et al. (1993); (7) Jobic et al. (1994).

## ACKNOWLEDGMENTS

W.H.P. is especially thankful to Guillermo Gimeno, Managing Director of Sunshine Argentina Inc., for generous support and hospitality at the mine site, and to his students K. Robl and G. Amann for excellent cooperation in the field. M.K. de B. is very grateful to Mario Tonel, formerly senior exploration geologist for Sunshine Argentina Inc., for providing the first samples with suredaite from Oploca. Moreover we want to express our gratitude to Emil Makovicky, Copenhagen, and Klaus Bente, Leipzig, for critical reviewing and their constructive comments, which greatly improved the manuscript. The authors extend their appreciation to Margit Ebner for patiently typing several versions of the manuscript, and to Winfried Waldhör for preparation of the polished sections. This investigation is part of a bilateral project ("Unconventional gold and silver deposits in NW-Argentina") between the Austrian Research Council (FWF, grant P13974GEO) and CONICET Argentina. Their financial support is gratefully acknowledged.

## REFERENCES CITED

- Altomare, A., Burla, M.C., Camalli, M., Cascarano, G., Giacobozzo, C., Guagliardi, A., and Polidori, G. (1994) SIR 92—a program for automatic solution of crystal structures by direct methods. *Journal of Applied Crystallography*, 27, 435.
- Amthauer, G., Fenner, J., Hafner, S., Holzapfel, W.B., and Keller, R. (1979) Effect of pressure on resistivity and Mössbauer spectra of the mixed valence compound Sn<sub>2</sub>S<sub>3</sub>. *Journal of Chemistry and Physics*, 70, 4837–4842.
- Angel, R.J., Allan, D.R., Miletich, R., and Finger, L.W. (1997) The use of quartz as an internal pressure standard in high pressure crystallography. *Journal of Applied Crystallography*, 30, 461–466.
- Anonymous (1997) Sunshine busca la plata de Piriquitas. *Latinoamerica* (Septiembre) 26, 75–77.
- Becker, P.J. and Coppens, P. (1974) Extinction within the limit of validity of the Darwin transfer equations. I. General formalisms for primary and secondary extinction and their application to spherical crystals. *Acta Crystallographica*, A30, 129–147.
- Blessing, R.H. (1987) Data reduction and error analysis for accurate single crystal diffraction intensities. *Crystallography Reviews*, 1, 3–58.
- Brasseur, H. and Pauling, L. (1938) The crystal structure of ammonium cadmium chloride, NH<sub>4</sub>CdCl<sub>3</sub>. *Journal of American Chemical Society*, 60, 2886–2890.
- Brown, I.D. and Shannon, R.D. (1973) Empirical bond-strength-bond-length curves for oxides. *Acta Crystallographica*, A29, 266–282.
- Burnham, C.W. (1966) Computation of absorption corrections and the significance of end effects. *American Mineralogist*, 51, 159–167.
- Chang, L.Y. and Brice, W.R. (1971) The herzenbergite-teallite series. *Mineralogical Magazine*, 38, 186–189.
- Coira, B.L. and Brodtkorb, M.K. de (1995) Polymetallic mineralization associated with Cenozoic volcanism in Northern Puna, Argentina. *Pacrim '95*, 135–140.
- Creagh, D.C. and McAuley, W.J. (1992) X-ray dispersion correction. In *AJC Wilson, Ed., International Tables for Crystallography, Volume C*, p 206–219. Kluwer, Dordrecht.
- Criddle, A.J. and Stanley, C.J. (1993) *The Quantitative Data File for Ore Minerals*, 635 p. Chapman and Hall, London.
- Finger, L.W. and Prince, E. (1975) A system of Fortran IV computer programs for crystal structure computations. U.S. National Bureau of Standards, Technical Note 854, 128 p.
- Grant, D.F. and Gabe, E.J. (1978) The analysis of single-crystal Bragg reflections from profile measurements. *Journal of Applied Crystallography*, 11, 114–120.
- Gressier, P., Meerschaut, A., and Rouxel, J. (1987) Structure determination and transport properties of a new phase with the approximate composition Sn<sub>1.2</sub>Ti<sub>0.8</sub>S<sub>3</sub>. *Materials Research Bulletin*, 22, 1573–1580.
- Huy-Dung, N., Etienne, J.E., and Laruelle, P. (1971) Isolement et structure cristalline d'une nouvelle famille de composés des terres rares de formule générale LCrSe<sub>3</sub> (L=La and Nd). *Bulletin de Societe Chimique Francaise*, 1971, 2433–2437.
- Jobic, S., Le Boterf, P., Bodenan, F., and Ouvard, G. (1994) Structure d'un nouveau sulfure ternaire de chrome: CrSbS<sub>3</sub>. *CR Academie Sciences*, 318, 893–900.
- Jumas, J.C., Ribes, M., Philippot, E., and Maurin, M. (1972) Sur le système (SnS<sub>2</sub>)(PbS). Structure cristalline de PbSnS<sub>3</sub>. *C.R. Academie Sciences*, 275, 267–272.
- King, H.E., and Finger, L.W. (1979) Diffracted beam crystal centering and its application to high-pressure crystallography. *Journal of Applied Crystallography*, 12, 374–378.
- Kniep, R., Mootz, D., Severin, U., and Wunderlich, H. (1982) Structure of Tin(II) Tin(IV) Trisulphide, a Redetermination. *Acta Crystallographica*, B38, 2022–2023.
- Lelieveld, R., and Ijdo, D.J.W. (1978) Lead Zirconium Sulphide. *Acta Crystallographica*, B34, 3348–3349.
- Lottermoser, W., Kaliba, P., Forcher, K., and Amthauer, G. (1993) MOESALZ: a computer program for the evaluation of Mössbauer spectra. University of Salzburg.
- Lutz, H.D., Engelen, B., Fischer, M., and Jung, M. (1988) Kristallstruktur sowie FIR- und Ramanspektren von GaCrSe<sub>3</sub>. *Zeitschrift für Anorganische und Allgemeine Chemie*, 566, 55–61.
- Malvicini, L. (1978) Las vetas de estaño y plata de mina Piriquitas (Pircas), prov. de Jujuy, Republica Argentina. *Revista de la Asociación Argentina de Mineralogía, Petrología y Sedimentología*, Rev. 9, 1–26.
- Mar, A. and Ibers, J.A. (1992) Structure of europium zirconium selenide, EuZrSe<sub>3</sub>. *Acta Crystallographica*, C48, 771–773.
- Maslen, E.N., Fox, A.G., and O'Keeffe, M.A. (1992) X-ray scattering. In: *AJC Wilson (ed) International Tables for Crystallography, Volume C*, p. 476–509. Kluwer Academic Publishers, Dordrecht.
- Meetsma, A., Wiegiers, A., Amthauer, G., and de Boer, J.L. (1993) Structure Determination of SnZrS<sub>3</sub>. *Acta Crystallographica*, C49, 2060–2062.
- Mootz, D. and Puhl, H. (1967) Die Kristallstruktur von Sn<sub>2</sub>S<sub>3</sub>. *Acta Crystallographica*, 23, 471–476.
- Paar, W.H., Brodtkorb, M.K. de, Topa, D., and Sureda, R.J. (1996) Caracterización mineralógica y química de algunas especies metalíferas de yacimiento Piriquitas, Provincia de Jujuy, República Argentina: Parte 1. XIII Congreso Geológico y III Congreso de Exploración de Hidrocarburos, Actas III: 159–172.
- Paulus, H. and Fuess, H. (1992) Crystal structure of indium antimony trisulfide, InSbS<sub>3</sub>. *Zeitschrift für Kristallographie*, 198, 125–126.
- Picot, P. and Johan, Z. (1982) *Atlas of Ore Minerals*. 458 p Elsevier, Amsterdam.
- Prior, G.T.A. (1904) On Teallite, a new sulphostannite of lead from Bolivia: and 1st relations to Franckeite and Cylindrite. *Mineralogical Magazine*, 14, 21–27.
- Pütz, W. (1979) Untersuchungen an Mischungen Pb<sub>1-x</sub>Sn<sub>1+x</sub>S<sub>3</sub>. Staatsarbeit Universität Düsseldorf. (Not seen: cited from Kniep, R., Mootz, D., Severin, U., and Wunderlich, H. (1982) *Acta Crystallographica*, B381, 2022–2023.)
- Ralph, R.L. and Finger, L.W. (1982) A computer program for refinement of crystal orientation matrix and lattice constants from diffractometer data with lattice symmetry constraints. *Journal of Applied Crystallography*, 15, 537–539.
- Stoe, and Cie (1994) VISUAL-X<sup>POW</sup>, Software Package for the Stoe Powder Diffraction System STADI P. Revised Version 2.27, July 1994. Stoe and Cie GmbH, Darmstadt, Germany.
- Sureda, R.J., Galliski, M.A., Argañaraz, P., and Daroca, J. (1986) Aspectos metalogénicos del noroeste argentino (provincias de Salta y Jujuy). *Capricornio*, 1, 39–96.
- Turner, J.C.M. (1982) Descripción Geológica de la hoja 3 ab, Mina Piriquitas. Ministerio de Economía, Servicio Geológico Nacional, Boletín No 187, 54 p.
- Wiegiers, G.A. Meetsma, A., Haange, R.J., and de Boer, J.L. (1989) Structure of Tin Hafnium Sulfide and Lead Hafnium Sulfide. *Acta Crystallographica*, C45, 847–849.

MANUSCRIPT RECEIVED JUNE 15, 1999

MANUSCRIPT ACCEPTED FEBRUARY 24, 2000

PAPER HANDLED BY GERALD GIESTER